New Zealand Journal of Geology and Geophysics

ISSN: (Print) (Online) Journal homepage: www.tandfonline.com/journals/tnzg20

Tsunami or storm deposit? A late Holocene sedimentary record from Swamp Bay, Rangitoto ki te Tonga/D'Urville Island, Aotearoa – New Zealand

Darren N. King, Kate Clark, Catherine Chagué, Xun Li, Emily Lane, Bruce G. McFadgen, Jarom Hippolite, Peter Meihana, Billy Wilson, John Dobson, Pene Geiger, Hamuera Robb, Daniel Hikuroa, Shaun Williams, Regine Morgenstern & Finn Scheele

To cite this article: Darren N. King, Kate Clark, Catherine Chagué, Xun Li, Emily Lane, Bruce G. McFadgen, Jarom Hippolite, Peter Meihana, Billy Wilson, John Dobson, Pene Geiger, Hamuera Robb, Daniel Hikuroa, Shaun Williams, Regine Morgenstern & Finn Scheele (2023) Tsunami or storm deposit? A late Holocene sedimentary record from Swamp Bay, Rangitoto ki te Tonga/D'Urville Island, Aotearoa – New Zealand, New Zealand Journal of Geology and Geophysics, 66:4, 629-645, DOI: 10.1080/00288306.2022.2087692

To link to this article: https://doi.org/10.1080/00288306.2022.2087692

Published online: 22 Jun 2022.

NEW ZEALAND JOURNAL OF GEOLOGY AND GEOPHYSICS
2023, VOL. 66, NO. 4, 629–645
https://doi.org/10.1080/00288306.2022.2087692

Taylor & Francis
Taylor & Francis Group

RESEARCH ARTICLE

OPEN ACCESS Check for updates

Tsunami or storm deposit? A late Holocene sedimentary record from Swamp Bay, Rangitoto ki te Tonga/D'Urville Island, Aotearoa – New Zealand

Darren N. King[a], Kate Clark[b], Catherine Chagué [c], Xun Li[b], Emily Lane [d], Bruce G. McFadgen[e], Jarom Hippolite[f], Peter Meihana[g], Billy Wilson[h], John Dobson[f], Pene Geiger[f], Hamuera Robb[h], Daniel Hikuroa [i], Shaun Williams [d], Regine Morgenstern[b] and Finn Scheele[b]

[a]National Institute of Water and Atmospheric Research (NIWA), Nelson, Aotearoa, New Zealand; [b]GNS Science, Wellington, New Zealand; [c]School of Biological, Earth and Environmental Sciences, UNSW Sydney, Sydney, Australia; [d]National Institute of Water and Atmospheric Research (NIWA), Christchurch, New Zealand; [e]Māori Studies, Victoria University of Wellington, Aotearoa, New Zealand; [f]Ngāti Koata Trust, Nelson, Aotearoa, New Zealand; [g]School of Humanities, Massey University, Aotearoa, New Zealand; [h]Te Rūnanga o Ngāti Kuia, Aotearoa, New Zealand; [i]Māori Studies, University of Auckland, Aotearoa, New Zealand

ABSTRACT

Informed by Māori oral histories that refer to past catastrophic marine inundations, multi-proxy analysis of stratigraphic records from Swamp Bay, Rangitoto ki te Tonga (D'Urville Island) shows evidence of an anomalous deposit extending some 160 m inland. The deposit includes two distinct lithofacies. The lower sand unit is inferred to have been transported from the marine environment, with corresponding increases in the percentages of benthic marine and brackish–marine diatoms, and geochemical properties indicative of sudden changes in environmental conditions. Radiocarbon dating indicates the deposit formation is less than 402 yrs BP, and pollen indicates it is unlikely to be younger than 1870 CE. Core stratigraphy age models and co-seismic chronologies point to the marine unit most likely being emplaced by tsunami transport associated with rupture of the Wairarapa Fault in 1855 CE. The overlying unit of gravel and silt is inferred to be fluvial deposit and slope-wash from the surrounding hills, loosened by ground-shaking following the earthquake. These findings indicate the 1855 CE earthquake may have been more complex than previously thought and, or, available tsunami modelling does not fully capture the local complexities in bathymetry and topography that can cause hazardous and localized tsunami amplification in embayments like Swamp Bay.

ARTICLE HISTORY
Received 21 December 2021
Accepted 6 June 2022

HANDLING EDITOR
Gabor Kereszturi

KEYWORDS
Māori; tsunami; earthquake; sedimentology; microfossils; geochemistry; Rangitoto ki te Tonga; D'Urville Island; Raukawa Moana; Cook Strait

Introduction and background

Coastal wetlands and lagoons are important physical environments for the preservation and investigation of deposits left by past tsunamis. Detailed stratigraphic studies have been conducted world-wide, and the resulting scholarship has contributed greatly to understanding the magnitude, sources and frequency of past events (e.g. Atwater 1987; Dawson et al. 1988; Minoura and Nakaya 1991; Moore et al. 1994; Goff et al. 2000; Cisternas et al. 2005; Monecke et al. 2008; De Martini et al. 2010; Ramírez-Herrera et al. 2012; Clark et al. 2015; Chagué et al. 2020). Many of these studies have also helped to improve the interpretation of tsunami-related signatures (often referred to as proxies) in sedimentary deposits, with multi-proxy analysis now established as a fundamental requirement for distinguishing palaeotsunami from anomalous fluvial- and/or coupled storm-wave- generated deposits (e.g. Tuttle et al. 2004; Morton et al. 2007; Chagué-Goff et al. 2011; Goff et al. 2012; Goto et al. 2015; Yap et al. 2021).

Recent inductive-based research in Aotearoa-New Zealand[1] (Aotearoa-NZ) alongside the Māori kin-groups of Ngāti Koata and Ngāti Kuia about ancestral experience with past tsunami(s) points to the potential for uncovering tsunami deposits on Rangitoto ki te Tonga (D'Urville Island) (King et al. 2018) (Figure 1). This active tectonic location situated within the greater Cook Strait region [Raukawa Moana] of central Aotearoa-NZ provides numerous sources for locally generated tsunamis, and given the country's oceanic setting it is also exposed to regionally and distantly generated tsunamis. The work presented here seeks to locate evidence of tsunami inundation(s) preserved within the wetland environment of Swamp Bay, Rangitoto ki te Tonga in order to estimate the age of any inferred past events, and to correlate any potential events with previous studies from across the region. The project also seeks to contribute to the active reclaiming of tribal histories surrounding past tsunami impacts, while simultaneously adding to scientific understandings of regional generating sources

CONTACT Darren N. King darren.king@niwa.co.nz
Supplemental data for this article can be accessed online at https://doi.org/10.1080/00288306.2022.2087692.

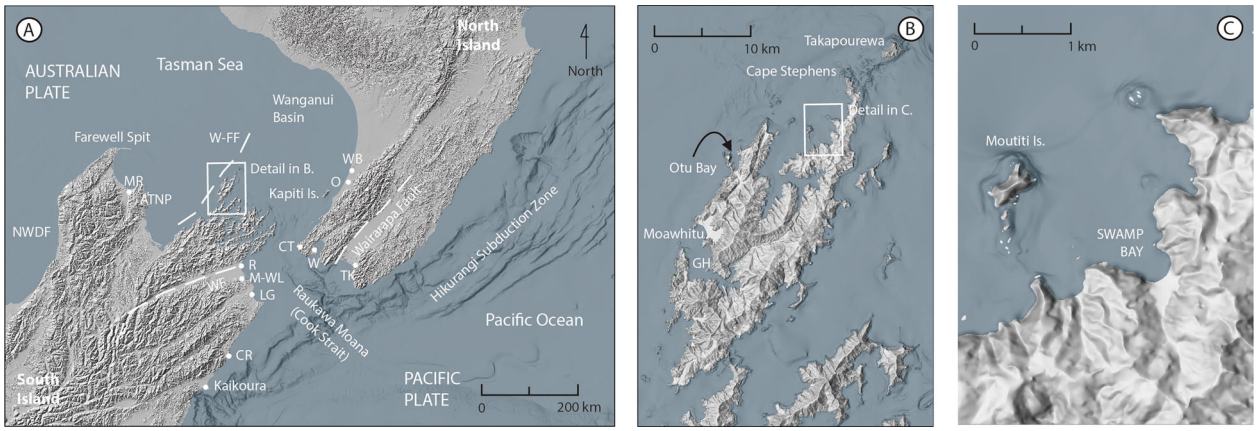

Figure 1. A, Tectonic setting of central Aotearoa-New Zealand and locations mentioned in the text. ATNP = Abel Tasman National Park, CT = Cape Terawhiti, CR = Clarence River, LG = Lake Grassmere, M-WL = Mataora-Wairau Lagoon, MR = Motupipi River, NWDF = North Westland deformation front, O = Otaki, R = Rarangi, TK = Te Kopi, WB = Waikawa Beach. **B**, Rangitoto ki te Tonga (D'Urville Island) and locations mentioned in the text. GH = Greville Harbour. **C**, Swamp Bay, Rangitoto ki te Tonga (D'Urville Island) and Moutiti Island.

and recurrence intervals for tsunamis across the top of the South Island, and the greater Cook Strait region.

Distinguishing tsunami deposits in onshore sedimentary records

Tsunamis can sometimes leave traces, or deposits, which, when preserved, can be used to detect past events. The most commonly used proxies to infer tsunami inundation are geological, including abrupt changes in sediment mineralogy and grain size (ranging from fine sediments to boulders), thinning or fining of sediments inland and upwards through a deposit, as well as sharp contacts between lithofacies that are typically erosional or unconformable in nature (e.g. Dawson and Shi 2000; Morton et al. 2007; Chagué-Goff et al. 2011; Goff et al. 2012). These characteristics are often complemented by the anomalous presence of intraclasts (rip-up clasts), shell, wood and other organics, as well as changes in microfossil assemblages such as diatoms, foraminifera and ostracods that signal disturbed habitats and altered environmental conditions (e.g. Hemphill-Haley 1996; Cisternas et al. 2005; Dura et al. 2016). Changes in chemical composition can also reflect variations in palaeosalinity, and/or minerals relative to under and overlying sediments (Chagué-Goff 2010; Chagué-Goff et al. 2017). In combination with these criteria, known local, regional and/or distant tsunamigenic sources, contemporaneous deposits at neighbouring sites, and archaeological information provide important contextual support for interpretations of past events (Atwater and Moore 1992; McFadgen and Goff 2007; Clark et al. 2015). Notwithstanding the importance of these tsunami signatures, the detection and confirmation of tsunami deposits depend strongly upon (i) the preservation potential of these deposits and the associated influence of post-depositional changes – e.g. long-term weathering, bioturbation, fluvial and marine reworking, and (ii) sufficient multi-proxy evidence to distinguish tsunami deposits from other sedimentary processes of transport and deposition in different receiving environments.

Environmental setting

Swamp Bay (40°45′S, 173°56′E) is located on the north-west coast of Rangitoto ki te Tonga (D'Urville Island), the northernmost island of the Marlborough Sounds, South Island, Aotearoa-New Zealand (Figure 1). The bay is a headland bound embayment characterised by steep hilly terrain amidst a drowned valley landscape (Johnston 1996). Covering an area of approximately 0.4 km^2, it is bounded along its coastal edge by a 200 m long sand-gravel beach ridge, which reaches a maximum elevation of ~6 m above mean sea level (amsl) in the south-west where it mantles the hillside (Figure 2). The elevation of the back-barrier wetland varies approximately 3-3.5 m amsl and increases in elevation gradually inland up the valley. Similar to other embayments across the region, the barrier most likely formed following the stabilisation of sea level some 7300–6500 years ago (e.g. Clement et al. 2016; Chagué et al. 2020; Kennedy et al. 2021), with a wetland developing behind it (Figure 2).

The surrounding hills of Swamp Bay range from 160 m to 360 m amsl. Their geology is dominated by ultramafic, mafic and sedimentary rocks, commonly enclosed in a serpentinite matrix, comprising the Patuki Melange (Johnston 1996). In contrast, the neighbouring Moutiti Island and the headlands to the west of Swamp Bay consist of metamorphosed sandstone and siltstone of the Matai Group (Johnston 1996).

Figure 2. **A**, Oblique view of Swamp Bay, Rangitoto (D'Urville Island) looking north across the embayment. (Photo source: Kate Clark). **B**, Oblique view of Swamp Bay, Rangitoto (D'Urville Island) looking south across the embayment. (Photo source: Kate Clark). **C**, Aerial view of the floatsam and debris washed into the wetland following Ex-Tropical Cyclone Gita in February 2018 (Photo source: Kate Clark). **D**, Beach-level view looking south across the embayment of storm wave and flood-carried debris following Ex-Tropical Cyclone Gita (Photo source: Gus Forgan). **E**, Location of vibracore site with grass-covered sand-gravel beach ridge in the background (Photo source: Rory Newsam). **F**, Beach-level view looking north across the embayment towards Moutiti (Victory Island) (Photo source: Bruce McFadgen).

Freshwater within Swamp Bay flows through a modified central gully system (cleared of native forest and drained for pastoral farming most likely sometime in the twentieth century), as well as through three smaller streams to the west and east. The salinity in the wetland varies from freshwater to brackish depending on recent rainfall, evaporation and/or flooding where coastal inundation is possible during storms. The wave climate of the bay is dominated by locally generated waves as well as long-period swell and storm waves from the north-west, with fetch lengths to the north and east severely restricted by the North Island. Ex-tropical Cyclone Gita at the end of February 2018, which severely impacted the upper South Island, resulted in flotsam and debris being washed into the wetland, with evidence of marine sediments carried by the storm waves reaching the top of the sand barrier (Figure 2).

Rangitoto ki te Tonga is located within a slowly subsiding tectonic block bounded by the Wairau Fault to the south, the Waimea–Flaxmore Fault system to the west and the Wanganui Basin to the north (Nicol 2011). The island lies within an area of moderate seismic hazard with active faults to the south east within Cook Strait [Raukawa Moana], east along the Kapiti-Manawatu Fault system (Nodder et al. 2007)

and west along the North Westland deformation front (Barnes and Ghisetti 2016). The Waimea-Flaxmore Fault system lies offshore to the west of Rangitoto ki te Tonga, but it is not known if this fault is active. The Hikurangi subduction zone lies to the east of Rangitoto ki te Tonga and the westward-subducting Pacific Plate lies at a depth of ~70 km below the study site (Williams et al. 2013).

Direct impacts from earthquakes on the Island most probably involve slope failures and rock-slides. Tsunami hazard and risk are also recognised, with Māori oral histories referring to a 'tidal wave' at Moawhitu (Greville Harbour) on the western side of the Island (Smith 1910; Mitchell and Mitchell 2004) and inductive-based research alongside the Māori kin-groups of Ngāti Koata and Ngāti Kuia indicating great waves striking and scouring the beach at the northern end of the Island (King et al. 2018). Marine pebbles on the surface of the Moawhitu sand barrier have been tentatively linked with a possible fifteenth century tsunami (McFadgen 2007) and more recently an inferred tsunami deposit was found within the Moawhitu wetland dating to ~2500-3000 yrs BP (Chagué et al. 2020), although storms cannot be ruled out unequivocally as a mechanism for transporting these deposits. Rangitoto ki te Tonga is also the location of some of the country's premier archaeological sites, comprising evidence of early- as well as late-period Māori occupation and trade (e.g. gardens, food storage pits, middens, fortifications, and argillite (pakohe) stone quarries) (Wellman 1962; Brailsford 1991; Patete 1997; Mitchell and Mitchell 2004).

Methods

Field methods

Following a reconnaissance visit in mid-February 2018, fieldwork was undertaken in April 2018 and November 2019. In April 2018, ten cores (SB-1 to SB-10) were extracted from the wetland area of Swamp Bay using a sediment vibracorer (Figure 3). When possible, cores were taken along transects perpendicular to the shore, with the furthest site 260 m inland from the active beach face. Their depths ranged between 1.58–3.89 m, with sediment compaction between 0.14–1.44 m (Supplementary data 1). Surveying was undertaken using a Real-Time Kinematic Global Positioning System (RTK-GPS) and an Unmanned Aerial Vehicle (UAV). Referencing for the UAV survey was provided by 10 ground control points measured with the RTK-GPS. All elevations are relative to the NZVD2016 vertical datum (in this area of New Zealand 0 m NZVD2016 is very close to mean sea level). All vibracore sites were surveyed using the RTK-GPS (precision ± 0.05 cm). Vibracore location coordinates, elevation, penetration depth and compaction information are provided in Supplementary data 1. Surface sediments were collected from the high- and low-tide limits as well as from the base of the surrounding hills to help with the interpretation of sediments from the extracted cores. In November 2019, a semi-cylindrical Eijkelkamp Gouge Auger was used to extract 31 cores from the north-eastern part of the wetland to trace the extent of a shallow sandy layer, with their location surveyed using a hand-held GPS (precision ± several metres) (Figure 3).

Analytical methods

All cores were split, photographed and described using the Troels-Smith classification system (Kershaw 1997). Based on the stratigraphy, core length, and spatial distribution cores SB-1, SB-2, SB-3 and SB-10 were selected for detailed sedimentological, mineralogical, geochemical, microfossil and geochronological (radiocarbon) analyses. Core logs for the ten cores extracted from Swamp Bay are provided in Supplementary data 2.

Samples for grain size analysis (n = 79) were taken at 20 cm intervals and at points immediately above, below and within visible stratigraphic changes. Sediments >1000 μm were sieved over 1_Φ intervals from 4 to 0 Φ and each fraction was weighed. The fraction <1000 μm was analysed using a Beckman Coulter LS13 320 Laser Diffraction Particle Size Analyser following treatment with hydrogen peroxide and sodium hexametaphosphate. These results were merged at equivalent 1_Φ intervals to enable the sand and gravel component to be included in the overall results. Gradistat Version 8 was used to process the results with geometric sample statistics presented (Blott and Pye 2001). In addition, selected samples from surface sediment as well as from key sedimentary units were examined under a binocular microscope to characterise their mineralogy.

Samples for diatom analysis taken from key stratigraphic units (n = 36) in cores SB-1, SB-2 and SB-3, were prepared following standard techniques (Battarbee 1986; Cochran 2002). Counts of 200–250 diatoms were made (where possible) using light microscopy at a magnification of ×1000. Species were identified based on standard diatom floras (Foged 1979; Krammer and Lange-Bertalot 1986, 1988, 1991a, 1991b; Round et al. 1990; Hartley 1996; Witkowski et al. 2000). They were then grouped according to salinity and habitat preferences following Round et al. (1990), Vos and de Wolf (1993), Van Dam et al. (1994) and Witkowski et al. (2000) to infer the palaeo-environmental significance of each sample and the potential source of the sediment.

ITRAX micro-XRF (X-Ray Fluorescence) scanning at the X-Ray Centre, University of Auckland was carried out at 1 mm intervals (with settings of 50 mA, 60

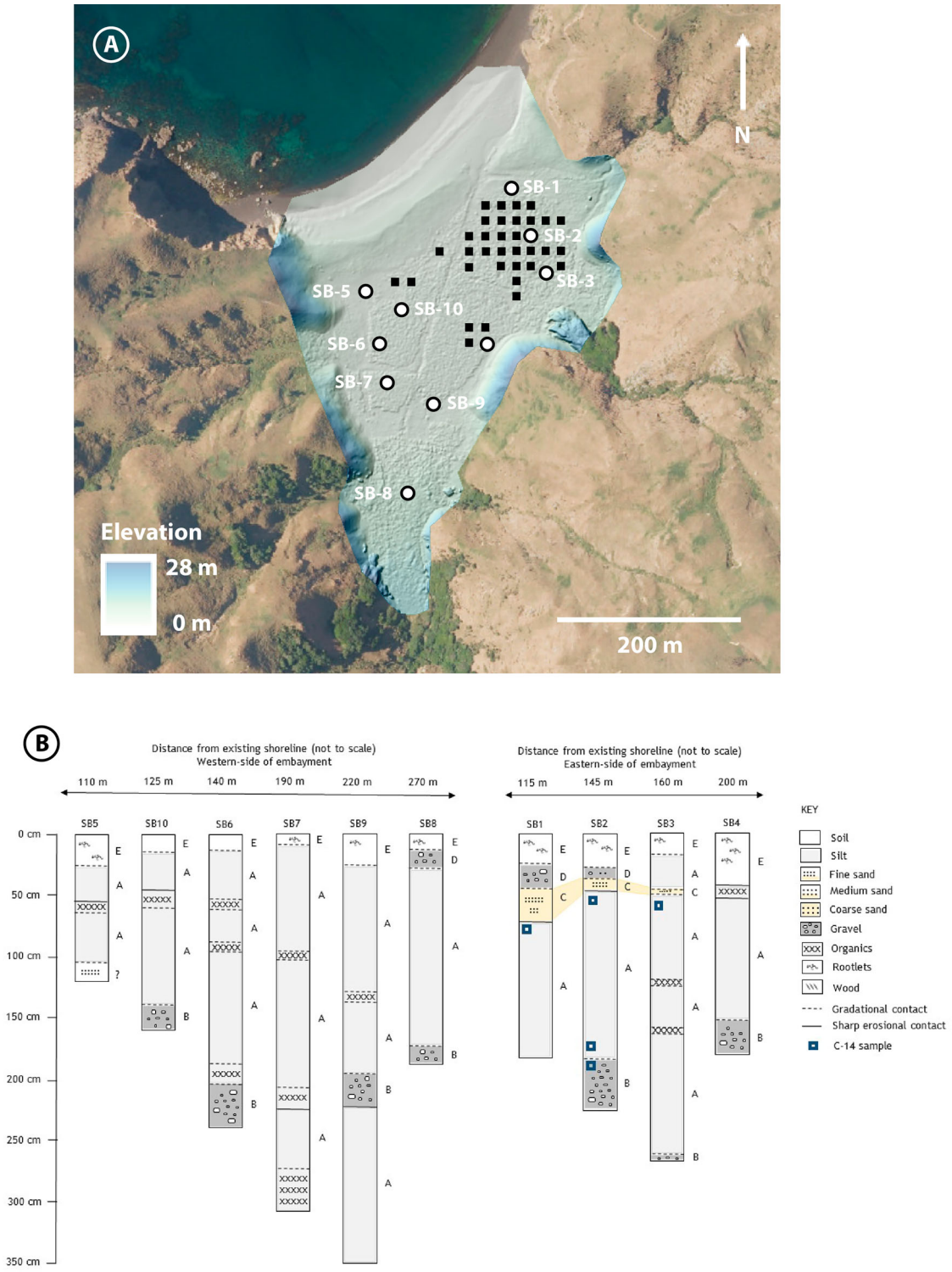

Figure 3. A, Location of vibracores (white circles with black outer circle) and gouge auger cores (black squares) Swamp Bay, Rangitoto (D'Urville Island) (Image source: Google-Earth-Pro 2020). A digital surface model derived from a Real-Time Kinematic Global Positioning System (RTK-GPS) and an Unmanned Aerial Vehicle (UAV) overlies the beach and wetland area of the embayment. Elevations are relative to mean sea level (NZVD2016 vertical datum). **B**, Transects illustrating surface topography and the generalised core stratigraphy and main lithofacies. Based on the sedimentary characteristics, sedimentary structures, grain size, and nature of contacts (depositional and/or erosional), the different lithological sections are classified into five units (a–e, from top to bottom). Vibracores are not to scale.

kV, 10 s exposure time) to provide a high-resolution elemental record. Elements known to assist lithostratigraphic analysis and the specific identification of signatures in association with marine inundation were selected in this study and were normalised over total counts (cps) (e.g. Croudace et al. 2006; Chagué-Goff et al. 2016). The ratio of incoherent vs coherent scattering data obtained with the molybdenum (Mo) tube of the instrument (reported as Mo R, also called Mo Inc/Mo Coh) was used as a proxy for organic

content as reported in previous studies (e.g. Guyard et al. 2007; Chagué-Goff et al. 2016). While it is acknowledged that the Mo R depends partly on moisture and type of organic matter, as inferred by Chawchai et al. (2016) and Woodward and Gadd (2019), it is regarded adequate for the purpose of this study, where we use semi-quantitative Itrax data as a tool to interpret environmental changes, in combination with other proxies. Principal component analysis (PCA) was also undertaken using the R studio v0.99.467 package to help interpret the relationships between different geochemical signatures and their varying organic, mineralogical and marine influences (e.g. Grunsky and Smee 1999; Chagué-Goff et al. 2016).

Samples for radiocarbon dating were taken from cores SB-1, SB-2, and SB-3 (n = 8) to provide chronological control for anomalous units and to help with correlation across cores. Standard acid-alkali-acid pre-treatment was used (Norris et al. 2020). Dated fractions included fragments of reeds and rootlets, unidentified plant material, charcoal and a wood fragment. They were analysed by accelerator mass spectrometry (AMS) at the Rafter Radiocarbon Laboratory, GNS Science, Wellington. Conventional radiocarbon ages (CRA) were calibrated to calendar years using the OxCal 4.3 programme (Bronk Ramsey 2009) against the SHCal13 calibration curve (Hogg et al. 2020).

To further probe the age of the anomalous units, seven sediment samples from SB-2 were analysed for dryland pollen with the intention of using the change in vegetation and presence of exotic (introduced) species to help constrain the chronology (Dunbar et al. 1997; Vandergoes et al. 2018). Samples were prepared following standard laboratory techniques (Faegri et al. 1989). Exotic *Lycopodium* tablets were added to each sample to allow the calculation of pollen concentrations. Pollen and spore identifications were made using standard texts (Pocknall 1981; Moar 1993) and the New Zealand pollen reference collections. Pollen data were presented in the form of relative frequency of a minimum pollen sum of 150 grains (if applicable). This sum includes pollen from all dryland plants (i.e. trees, shrubs and herbaceous plants). Pollen of other groups (wetland, aquatics, ferns, tree ferns) were excluded from the pollen sum, but their percentages were calculated as a proportion of dryland pollen, plus the respective group. Charcoal particles were also counted during pollen counting as number of fragments and presented as concentration per cm^3.

Results and interpretations

The lithostratigraphy across all vibracores comprises varying sedimentary units of silt, organics, sand, gravel and soil (Figure 3 and Supplementary data 2). However, cores SB-1 and SB-2 also comprise an anomalous deposit made up of two distinct lithofacies including a chaotic matrix of gravel and silts overlying coarse sand and pebbles within wetland muds and soil. Given the primary intent of this study to locate deposits of possible tsunami origin, we focus attention on cores SB-1 and SB-2 (Figures 4 and 5), and to a lesser extent SB-3 (Supplementary data 3) where traces of the anomalous unit are also present. Based on the sedimentary characteristics and structures, grain size, and nature of contacts (depositional and/or erosional), the different lithological sections are classified into five units (A–E, from bottom to top) and reported below. Diatom lifeform and salinity data as well as geochemistry from cores SB-1, SB-2 and SB-3 are also described for each lithofacies. Supplementary Data 4 provides raw counts of the full diatom flora (n = 123 species) identified from Swamp Bay. Supplementary data 5 provides information about the taxa names, morphological characteristics, salinity and habitat preferences.

Lithostratigraphy, diatoms and geochemistry

Lithofacies A is present in all cores and comprises a silty matrix with varying amounts of organic content (Figure 3 and Supplementary data 2). The silty nature of this lithofacies is associated with a generally higher and variable organic content, as shown by the proxy Mo R in Figures 4 and 5. The diatom assemblage in SB-1 is dominated by freshwater (salt intolerant) and fresh-brackish (somewhat tolerant of salt) taxa with high percentage counts of the benthic lifeforms *Cavernosa kapitiana, Luticola mutica, Nitzschia amphibia* and *Orthoseira roseana* as well as the aerophylic lifeforms *Hantzschia amphioxys* and *Humidophila contenta.* This assemblage is highly consistent with the taxa identified from samples taken from SB-2 and SB-3 within this lithofacies, although high percentage counts of the benthic fresh-water species *Cocconeis placentula var. euglypta* also occur in both cores. In all three cores there are notable background percentages of the brackish–marine diatom *Paralia sulcata.*

Lithofacies B is the basal unit in core SB-2 and SB-3, and comprises a poorly sorted coarse-gravel with angular clasts (0.5-4 cm diameter). While not present in SB-1 (most likely due to insufficient penetration depth of the core) it occurs in most cores extracted from across the embayment (Figure 3 and Supplementary data 2). The main chemical characteristics (in SB-2) are high counts of Ca/cps, Fe/cps and Ti/cps. The organic content is low, as reflected in low Mo R (Figure 5). Samples taken from this lithofacies in core SB-2 (180 and 200 cm depth) returned very low diatom counts (n = <50) with most of the taxa counted unidentifiable as they were ill-preserved, resting in

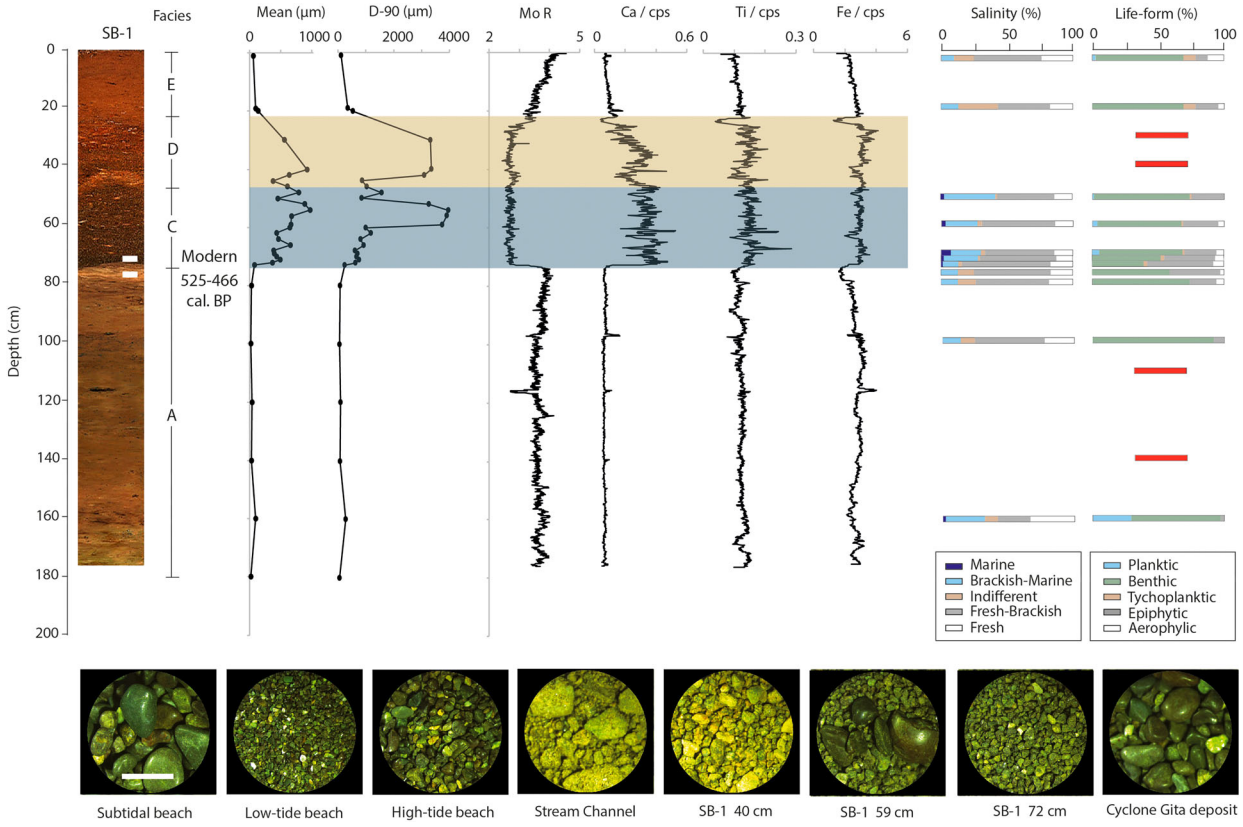

Figure 4. Optical image of core SB-1 with radiocarbon age (cal. yr. BP), mean and D-90 grain-size statistics, and elemental profiles from ITRAX scanning for molybdenum Incoherent/ Coherent ratio (Mo R), calcium (Ca / cps), titanium (Ti / cps) and iron (Fe / cps). The elemental data are displayed as counts normalised by counts per second (cps). Diatom salinity and lifeform preferences are also presented. No diatoms were observed in samples taken from 30, 40, 110 and 140 cm depth. The inferred marine and alluvial disturbance units are shaded grey blue and light brown, respectively. Photomicrographs illustrate the sedimentary composition of samples taken from the modern beach, stream channel, the top of the barrier - cyclone Gita deposit, as well as 40 , 59 and 72 cm depth in SB-1. Scale bar (white line) = 0.5 cm.

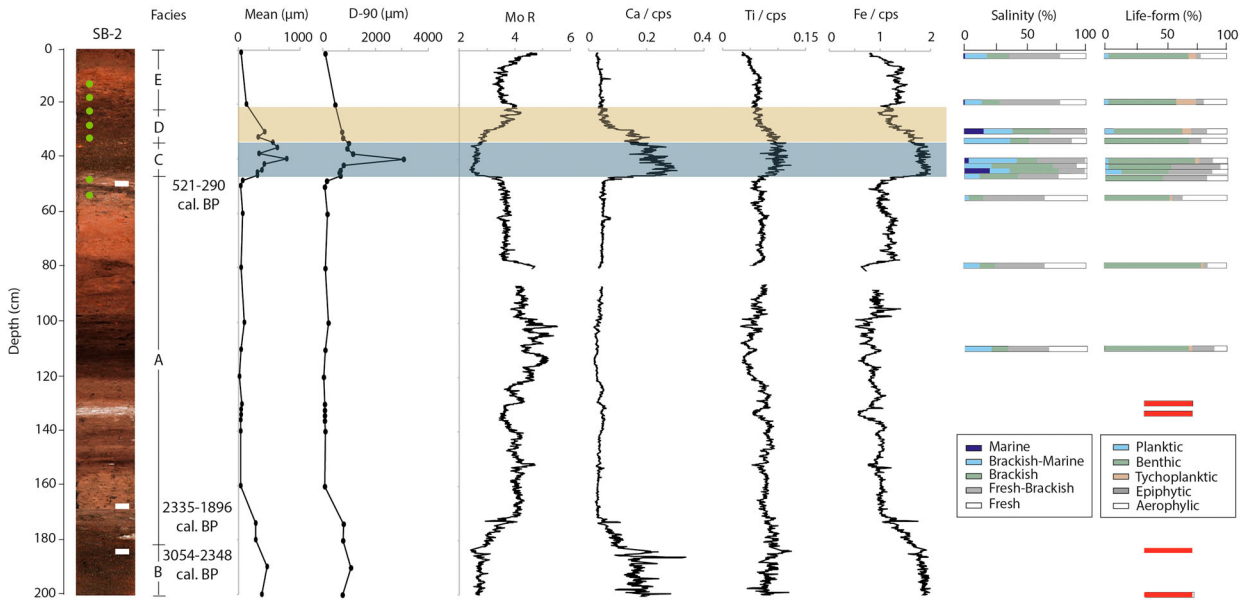

Figure 5. Optical image of core SB-2 with radiocarbon age (cal. yr. BP), mean and D-90 grain-size statistics, elemental profiles from ITRAX scanning for molybdenum Incoherent/ Coherent ratio (Mo R), calcium (Ca / cps), titanium (Ti / cps) and iron (Fe / cps), diatom salinity and lifeform preferences. The elemental data are displayed as counts normalised by counts per second (cps). No diatoms were observed in samples taken from 130 and 140 cm depth. The green dots indicate the sampling positions for pollen analysis. Defined by peaks in selected grain size, elemental composition and diatom data the inferred marine and alluvial disturbance units are shaded grey blue and light brown, respectively. The dashed box denotes the inferred former beach surface.

girdle view, or because the valves were obscured by fine overlying material.

Lithofacies C comprises a medium to coarse sand with discrete occurrences of rounded pebbles (<5 cm diameter), scattered plant rootlets and mud rip-up clasts (from lithofacies A), displaying a sharp and erosional lower contact in SB-1 and SB-2. In SB-1 this lithofacies occurs at 73–46 cm depth, with the mean grain-size increasing from 77 μm at 73 cm to a peak of 969 μm at 54 cm depth, then decreasing upwards through the sedimentary unit to a gradational upper contact at 46 cm depth. This pattern is repeated in SB-2 where this lithofacies lies at 47–37 cm depth. The mean grain-size in SB-2 increases sharply from 305 μm at 47 cm to a peak of 783 μm at 40 cm, before also fining upwards through the sedimentary unit to the gradational upper contact at 37 cm depth. A trace of this lithofacies is also present in SB-3 (50–46 cm depth), where the mean grain size ranges from 27 to 90 μm. Lithofacies C is dominated by a highly mixed assemblage of diatom taxa. In both SB-1 and SB-2 there are high percentage counts in benthic marine species (e.g. *Pseudopodosira kosugii* and *Ehrenbergiulva granulosa*) and benthic brackish–marine species (e.g. *Paralia sulcata, Diploneis smithii* and *Melosira nummuloides*). Fresh-brackish and freshwater taxa are also common with comparatively high percentage counts of the benthic lifeforms *Luticola mutica, Nitzschia amphibia*, *Nitzschia terrestris, Pinnularia obscura, Pinnularia viridis* and *Rhopalodia novae zealandiae* as well as the aerophylic lifeforms *Hantzschia amphioxys* and *Humidophila contenta.* The marine and brackish–marine signal declines upwards through this sedimentary unit as it transitions into lithofacies D. Lithofacies C is also characterised by a marked and sharp increase in Ca/cps, Ti/cps and Fe/cps counts that correlates with a decrease in Mo R (organic content) compared to lithofacies A.

Lithofacies D is a very poorly sorted gravel and silt sedimentary unit comprising angular and sub-angular clasts (<5 cm diameter), iron oxides and scattered plant rootlets. The lower contact is gradational across SB-1 (46 −24 cm depth) and SB-2 (37–26 cm depth), with the mean grain size ranging from 372 to 917 μm in SB-1 and 321–426 μm in SB-2. The upper contact of this lithofacies in both cores is gradational. Diatoms were absent from the samples taken in SB-1. However, in SB-2 the diatom assemblage was dominated by freshwater and fresh-brackish taxa with >50% of the total assemblage benthic lifeforms such as Rhoicosphenia abbreviata, *Pinnularia obscura, Luticola mutica, Rhopalodia musculus, Stauroneis kriegeri* and Surirella brebissonii and approximately 14% of the total assemblage aerophylic lifeforms such as *Hantzschia amphioxys* and *Humidophila contenta*. Notwithstanding these distributions, some 30% of the assemblage comprised the benthic brackish–marine species *Paralia sulcata* and *Diploneis smithii.* The chemical characteristics of lithofacies D are somewhat similar to those of lithofacies C, with high counts in Ca/cps, Ti/cps and Fe/cps, although they display some spatial variations, reflecting the variable organic content, as shown in core SB-2 (Figure 5).

Lithofacies E caps the stratigraphic sequence in SB-1, SB-2 and SB-3. It comprises medium brown soil and surface organics associated with salt marsh, saltwort and salt meadow vegetation (Figure 3 and Supplementary data 2). It is present across most cores extracted from the wetland and overlies the chaotic gravel and silts of lithofacies D. It is dominated by benthic, tychoplanktic and aerophylic lifeforms with strong preferences (60-75% of the total diatom assemblage across SB-1, SB-2 and SB-3) for freshwater and fresh-brackish salinity conditions – e.g. *Hantzschia amphioxys, Humidophila contenta*, *Luticola mutica*, *Pinnularia viridis, Rhoicosphenia abbreviata* and *Staurosirella pinnata*. However, at the surface of all three cores there is also a significant brackish–marine salinity signal (10-20% of the total assemblage) which is dominated by the presence of the littoral species *Paralia sulcata*. The organic content exhibits some variations, which are inversely correlated with variations in Ca/cps, Ti/cps and Fe/cps.

Principal component analysis (PCA) of the geochemical data from cores SB-1, SB-2 and SB-3, shows that between 40% (SB-2) and nearly 68% (SB-3) of the variance between different facies can be explained by the first two components (Figure 6). These statistics also distinguish the source material of the different lithofacies (based on mineralogical characteristics reflected in the chemical composition) described in the sedimentary sequences.

Geochronology and pollen

Given the number of proxies that indicated lithofacies C was from a marine source, we targeted this unit using radiocarbon dating and palynology techniques to constrain the timing of its deposition. We selected samples for radiocarbon analysis from immediately below, within and above lithofacies C in SB-1 and SB-2, and we also selected samples from deeper in SB-2 to understand the broader sediment accumulation rates in the valley. In total, 6 samples were taken from SB-1, 9 samples from SB-2, and 2 samples from SB-3, to help cross-correlate between cores. Of these 17 samples, only 8 contained a viable amount of terrestrial organic material for radiocarbon dating. The radiocarbon results are reported in Table 1. We refer to calibrated radiocarbon ages, which are presented as year before present (BP), with 'present' defined as 1950 CE. Many of the calibrated radiocarbon ages (2-sigma) have relatively large uncertainties

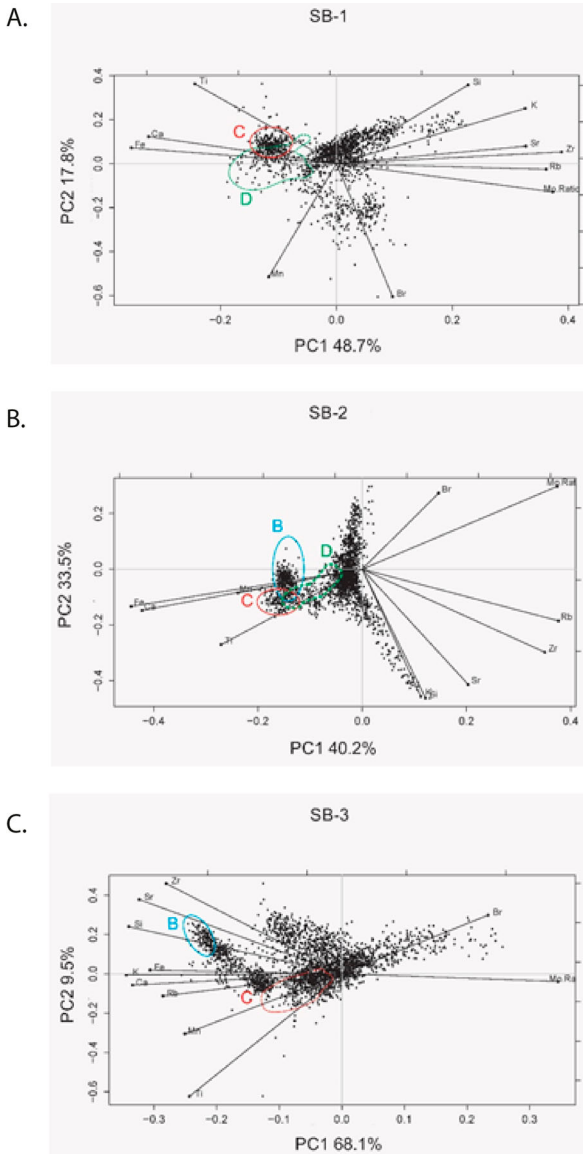

Figure 6. Bi-plots of the first two principal components among the set of 10 geochemical variables for SB-1 (Figure A), SB-2 (Figure B) and SB-3 (Figure C). The direction and length of the vector indicate how each variable contributes to the two principal components. The notation 'B' = the basal unit in core SB-2 and SB-3 comprising a poorly sorted coarse gravel with angular clasts. The notation 'C' = the inferred marine unit comprising a well-sorted medium to coarse sand with discrete occurrences of rounded pebbles. The notation 'D' = the inferred fluvial unit comprising very poorly sorted gravel and silts with angular and sub-angular clasts.

due to the small size of the samples collected (up to ± 204 yrs).

Overall, the ages provide approximate chronological succession throughout the stratigraphic profiles of the cores sampled, as well as cross-correlations between cores. Age constraint on lithofacies C is provided by three calibrated radiocarbon ages underlying the deposit at 74–75 cm (525-466 yrs BP, NZA41216/2) in SB-1, 47–48 cm (521-290 yrs BP, NZA41216/4) in SB-2 and 48–49 cm (1372 yrs BP, NZA41265/7) in SB-3 (Table 1). While the closeness and overlap of two of these ages suggest that they are from the same deposit, the overlap does not necessarily indicate good evidence that there is minimal inbuilt age (McFadgen 1982). That is, wood and charcoal can carry in-built age either from the tree-ring age of the wood, or possibly as a result of reworking of the sample from local sources, or both (McFadgen 2007). One or both of these scenarios is likely to be the case for the significantly older calibrated radiocarbon age obtained from 48–49 cm in SB-3. Meanwhile, modern radiocarbon ages (ages with a calibrated age range extending younger than AD 1950) at 58–59 cm and 70–71 cm depth in SB-2, suggests that they are from younger material moved deeper into the wetland sediments by bioturbation. Further, another modern radiocarbon age from within the anomalous deposit at 71–72 cm depth in SB-1 either reflects modern carbon being shifted deeper into the sediment due to plant roots or bioturbation, or alternatively a more recent age for the anomalous deposit. Notwithstanding these uncertainties, the younger of the three samples from beneath lithofacies C provides a maximum date of 402 yrs BP for the emplacement of this anomalous deposit (i.e. the deposit is less than 402 yrs BP).

To further probe the age of lithofacies C, we investigated the pollen assemblage of the sediments below and above the marine deposit (Figure 5 and 7). Pollen preserved in sediment can show distinctive changes in vegetation that reflect the presence and timing of Māori and European settlement (McGlone 1989; Elliot et al. 1995; Chester and Prior 2004; McGlone et al. 2005; Vandergoes et al. 2018). Seven samples from SB-2 were studied for palynology: two from below lithofacies C, and five from above Lithofacies C (Figure 5 and 7).

The samples at 48 and 55 cm (both below Lithofacies C) have high frequencies of *Pteridium esculentum* along with high charcoal concentrations (normally an indicator of Māori occupation and a decline in tall tree pollen - e.g. Elliot et al. 1995). In addition, the high frequencies of tree fern *Cyathea* types at 48 and 55 cm suggest either a recovery state from deforestation, since the tree fern often acts as a nursery plant (Brownsey and Smith-Dodsworth 2000), or that the fern spores were washed-in from inland as a result of land clearing as they are typically more resistant than pollen grains (especially oxidising conditions) (Reitz and Shackley 2012). Whatever the case might be, both scenarios are consistent with Māori using and/or occupying the area prior to the emplacement of lithofacies C. This interpretation is also consistent with the calibrated radiocarbon age of 402 yrs BP at 48–49 cm from SB-2. Meanwhile, in the samples collected above lithofacies C, exotic pollen grains such as *Pinus* and *Rumex acetocella* (sheep sorrel) were observed within lithofacies E (at 15 , 20 and 25 cm) along with pasture components such as grass and *Taraxacum*. The appearance of these exotic pollens is

Table 1. Radiocarbon ages for Swamp Bay, Rangitoto ki te Tonga (D'Urville Island), Aotearoa-New Zealand. CRA = Conventional Radiocarbon Age, CRA – Convention radiocarbon ages were completed using OxCal 4.3 (Bronk Ramsey 2009) and the Southern Hemisphere calibration curve SHCal13 (Hogg et al. 2020). BP = Before CE 1950, F = fraction modern, Modern = ages with a calibrated age range extending younger than AD 1950.

Vibracore ID	Sample depth (cm)	Material dated	Rafter laboratory ID	NZA	CRA (Years BP 1σ)	CRA error	F	F error	$\Delta^{14}C$ (‰)	$\Delta^{14}C$ error	Calibrated Age Range (Cal. years BP, 95%)
SB-1	71–72	Organic rich sediment	NZA41216/1	66227	Modern	–	1.115461	0.018264	106.29	18.11	Modern
SB-1	74–75	Charcoal (species unknown)	NZA41216/2	65840	479	21	0.9421	0.0024	−65.6	2.4	525–466
SB-2	47–48	Charcoal (species unknown)	NZA41216/4	66228	402	72	0.9512	0.0086	−56.6	8.5	521–290
SB-2	58–59	Organic rich sediment	NZA41265/4	67294	294	204	0.963983	0.024573	–	–	622-Modern
SB-2	70–71	Organic rich sediment	NZA41265/5	67295	Modern	–	1.109118	0.002635	–	–	Modern
SB-2	170–171	Organic rich sediment	NZA41216/5	66229	2205	96	0.7599	0.0091	−246.4	9.1	2355–1896
SB-2	185–186	Organic rich sediment	NZA41216/6	66230	2654	130	0.7186	0.0117	−287.3	11.6	3054–2348
SB-3	48–49	Wood (species unknown)	NZA41265/7	67296	1372	20	0.842899	0.002118	–	–	1296–1177

most likely associated with land clearance following gradual settlement of the Island by Europeans after 1840 CE (Patete 1997). However, given that *Rumex acetocella* was first recorded in Aotearoa-NZ in 1867 (Moore 1955) and that *Pinus* was beginning to spread across the country by the 1890s (Webb et al. 1988; Wardle 1991), we estimate the timing of the introduction and distribution of these exotic pollens into the sedimentary record on Rangitoto ki te Tonga is most likely to be post-1870 CE at the earliest. This indicates that both lithofacies C and D are very unlikely to be younger than 1870 CE.

Discussion

Palaeoenvironmental changes

The lithostratigraphy, geochemistry and microfossil assemblages from the cores collected from Swamp Bay indicate a spatially variable history of late-Holocene environmental conditions. While the different lithofacies A–E can be broadly correlated across the study area, there are notable anomalies in the cores SB-1, SB-2 and SB-3 that emphasise five distinct modes of sedimentation. Interpretation of the paleoenvironmental record is provided below, with emphasis given to the evidence collected from cores SB-1 and SB-2. References are made to other cores when correlations and/or exceptions are noteworthy.

Lithofacies A is ubiquitous across the wetland environment of Swamp Bay, and is interpreted as representing in-situ accumulation in standing and/or ephemeral wetland waters with some input from the surrounding catchment. The diatom assemblage within this lithofacies (based on SB-1 and SB-2) is dominated by freshwater (salt intolerant) and fresh-brackish (somewhat tolerant of salt) benthic and aerophylic lifeforms signalling a terrestrial aquatic environment favouring diatom growth and preservation. The aerophylic lifeforms are commonly sourced from eroded soils (Round et al. 1990; Tanigawa et al. 2018). Collectively, these indicators are consistent with a low-energy back-barrier wetland environment.

Importantly, it was not possible to define the base of lithofacies A (Figure 3 and Supplementary data 2) and thereby we are unable to provide reliable age control on the development of the wetland. The formation of the gravel barrier, presumably sometime following the onset of sea-level stillstand circa 7.5 ka, using the SW North Island sea-level curve from Clement et al. (2016), would have effectively sealed the back-barrier area of the embayment from regular marine influences thereby facilitating conditions suitable for freshwater wetland development. This interpretation is consistent with the timing of the barrier formation at Moawhitu (circa 7.3 ka), ~20 km SSW of Swamp Bay (Chagué et al. 2020). Consequently, we interpret lithofacies A as developing after the formation of the gravel barrier, which was probably established between 7.5 and 4 ka when sea-level began to fall from the mid-Holocene high-stand (Clement et al. 2016). It is also notable that lithofacies A comprises multiple phases of high organic content (Mo R, Figures 4 and 5) which is consistent with the episodic production and accumulation of in-situ organics, much like the modern environment.

Lithofacies B comprises a poorly sorted coarse-gravel with angular clasts. Its presence across most cores points to a possible embayment-wide disturbance event (Figures 3 and 4, and Supplementary data

2). The organic content of this lithofacies is low as reflected in low Mo R ratios in SB-1 and SB-2 (Figures 4 and 5), and those diatom taxa that were counted were mainly unidentifiable most likely due to dissolution through secondary and tertiary geochemical processes (Denys and de Wolf 1999; Cochran 2002). Further, the lower contact of this lithofacies (visible in core SB-9 only) is erosional. While it was not possible to penetrate beneath lithofacies B in all other cores, these clastic-dominated sediments coupled with a decrease in bulk organic content are interpreted as flood deposits from alluvial sources that subsequently transition back to gradual processes of sedimentation as outlined above for lithofacies A. The tight distribution of the principal components of lithofacies B in SB-2 and SB-3 suggests it is from a single source with little mixing with the receiving environment (see PCA: Figure 6)

Lithofacies C is characterised by a sharp transition to medium to coarse sand with discrete occurrences of well-rounded pebbles (<5 cm diameter), scattered plant rootlets and mud rip-up clasts. The coarse sand granules and rounded clasts bear a strong similarity to the green and grey sandstone, with traces of quartzite and chert, which dominate the modern-day beach (Figure 4). Furthermore, the medium to coarse sand contrasts strongly with the angular clasts in the modern stream bed. Lithofacies C is also marked by a highly mixed assemblage of diatom taxa where percentage counts of benthic marine and brackish–marine species are notably higher than any of the lithofacies above or below this sedimentary unit. There is also a sharp increase in Ca/cps, Ti/Cps and Fe/cps (Figures 3, 4 and Supplementary Data 3) in this lithofacies which is most likely associated with the distinct mineralogy of the allochthonous material (possibly from metamorphosed sandstone and siltstone of the Matai group) brought in during marine inundation (e.g. Chagué-Goff et al. 2015). While an increase in Ca is often linked to the presence of shells (carbonates), no shell/shell hash was observed in lithofacies C. The small scatter of datapoints for lithofacies C in PCA (Figure 6) is interpreted as representing a specific source material, such as the beach, as also reflected in the composition of the sediment. Collectively these changes suggest that the wetland at Swamp Bay underwent a sudden influx of seawater and marine sediment before being covered by lithofacies D. We thereby interpret lithofacies C as marine-derived and from this point refer to lithofacies C as a 'marine deposit'. It is also noteworthy that based on the presence of exotic pollen grains such as *Pinus* and *Rumex acetocella* along with pasture components such as grass and *Taraxacum* in samples taken from lithofacies E in SB-2 it is very unlikely that the marine deposit (lithofacies C) can be younger than 1870 CE.

Following the inferred marine incursion represented by lithofacies C in SB-1, SB-2 and SB-3, there is a stark change in the overlying lithofacies D. The lithology is made up of very poorly sorted gravel and silt comprising angular and sub-angular clasts (<5 cm diameter), iron oxides most likely due to prolonged weathering of the shattered rock, and scattered plant rootlets. This lithofacies is present in SB-1 and SB-2, as well as SB-8 (Supplementary data 2), but not SB-3. While the chemical characteristics of lithofacies D are somewhat similar to those of lithofacies C, there is a higher organic content in lithofacies D, as reflected in an upward increase in Mo R, which very likely reflects terrestrial input. The wide distribution of principal components confirms the incorporation of material from multiple sources (see PCA: Figure 6) (Chagué-Goff et al. 2015). This lithofacies is comparable to the gravel and angular clasts found in lithofacies B and is interpreted as a mixed deposit of fluvial material and slope wash from the surrounding hills transported across the wetland during run-off events. The uneven spatial distribution of this lithofacies is interpreted as reflecting the principal gully streams as sources for these deposits.

The most recent phase of sedimentation (lithofacies E) comprises the development of medium brown soil in association with salt marsh surface organics and partial drainage of the wetland for pastoral farming (date unknown).

Origin and timing of the anomalous marine deposit

Only three vibracores contained sediments consistent with a marine incursion into the Swamp Bay wetland. These were the two most seaward cores SB-1 and SB-2, and SB-3 where the inferred marine deposit (lithofacies C) is present at 50–46 cm depth (Supplementary data 3). Given the presence of marine diatoms in the deposit, terrestrial flooding of the embayment is not considered a credible emplacement mechanism. However, two processes are capable of transporting marine sands into the Swamp Bay wetland, namely (i) coastal storm and flooding possibly coincident with high tides, and (ii) tsunami generated by an earthquake and/or local submarine landslides. To help understand the character of the marine deposit and unravel the process that most likely caused its deposition we mapped its extent using a dense network of gouge auger cores (Figures 7–8). The marine deposit is limited to the eastern side of the wetland extending up to 160 m inland from the modern high-tide line (Figure 4 and 5, and Supplementary data 3). The deposit is thicker near the barrier and thins inland with a corresponding decrease in the mean and D-90 grainsize statistics. These spatial features indicate the marine

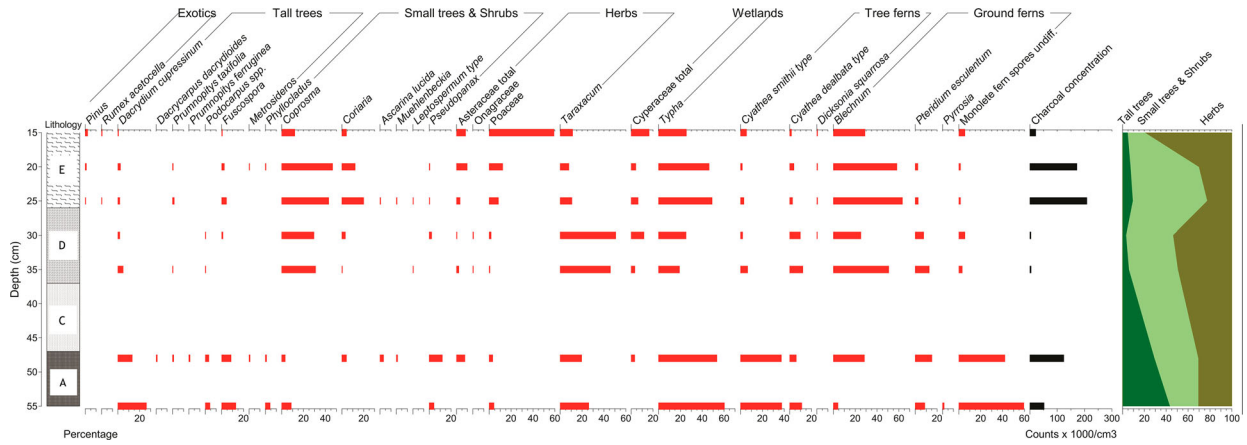

Figure 7. Pollen composition from samples taken from SB-2 bounding lithofacies C - the inferred marine overwash. Refer to Figures 4 and 5 for the positions of these pollen analyses.

deposit was most likely transported into the backbarrier zone through the stream channel, rather than directly over the barrier. The extent of the marine deposit is also considerably greater than the extent of sediments deposited on top of the barrier during the storm surge of ex-Tropical Cyclone (TC) Gita (Figure 2 and 9). No marine sediments were detected within the wetland from ex-TC Gita (Figure 8). While we cannot be sure that ex-TC Gita is characteristic of the largest storm surge to impact Rangitoto ki te Tonga (see Synoptic charts: Supplementary data 6) and a simple measure of distance inland is not a sufficient criterion for differentiating between storm and tsunami deposits, the clear mismatch between the known frequency of high-magnitude storm events in and around the north of the South Island (Pascoe 1983) and the corresponding absence of other marine deposits (other than lithofacies C) in the stratigraphic record suggests that the wetland has very likely remained isolated from episodic storm surges for at least ~2000 years.

Figure 8. The extent of the marine overwash deposit (blue circles) and the location of discrete deposits from ex-Tropical Cyclone Gita (red patches) at Swamp Bay, Rangitoto (D'Urville Island).

One of the most important criterion for inferring tsunami transport of marine sediments is to establish a link with a tsunami generating source, either directly from stratigraphic evidence of vertical deformation caused by an earthquake (i.e. co-seismic subsidence) and/or from contemporaneous deposits preserved within sedimentary layers at neighbouring sites. Radiocarbon dating indicates a maximum date of 402 yrs BP for the timing of the marine deposit (lithofacies C) at Swamp Bay, although it could be considerably younger due to in-built age. Meanwhile, palynology indicates that it is very unlikely that the marine deposit can be younger than 1870 CE. The most significant tsunami to impact the greater Cook Strait region during this period occurred on 23 January 1855 CE following the MW 8.2 rupture of the onshore-offshore Wairarapa fault east of Wellington (Grapes and Downes 1997; Downes 2015). According to the New Zealand Historic Tsunami Database (NZHTDB) the highest tsunami run-up heights from this earthquake rupture were equal to or greater than 10 m at Te Kopi in eastern Palliser Bay (Downes 2015). Waves were also observed sweeping across Lyall Bay and Evans Bay to reach some 2-2.5 km inland to what is now the suburb of Miramar, and waves were recorded at least as far north as Waikawa Beach near Otaki where fish were deposited above the high-water mark (Downes 2015). On the southern shore of Cook Strait the effects of the 1855 CE tsunami were observed along the Wairau Bar (run-up probably reaching 6–7 m near Rarangi Beach) (Downes 2015), and a detailed description of the forceful impact of the earthquake and tsunami on the western side of Cook Strait at Farewell Spit is provided in a recently uncovered newspaper report from the Auckland Star in 1894 (Supplementary data 7). Collectively, these records

reveal that the 1855 CE earthquake generated tsunami waves that significantly affected the entire Cook Strait region.

To test the tsunami deposit hypothesis presented here we modelled the likely maximum tsunami height at Swamp Bay generated by rupture of the Wairarapa Fault in the 1855 CE Mw 8.2 earthquake (Figure 9). Tsunami modelling was conducted using Basilisk (Popinet 2011; 2015) and the source model adapted from Mueller and Power (2014) for the earthquake deformation. The model simulation shows tsunami heights that are consistent with historic observations near the rupture zone, however it is evident that tsunami heights to the west and across the northern embayments of Rangitoto ki te Tonga are negligible, which is inconsistent with the sedimentary evidence preserved at Swamp Bay. Notwithstanding these differences, we understand that there are a range of factors that influence the deposition and preservation of tsunami deposits including the direction of tsunami inundation, tide level and sediment availability.

It is feasible that rupture of the Wairarapa Fault in 1855 CE might have included slip on the Hikurangi subduction interface (Beavan and Darby 2005; Clark et al. 2015), as well as potential rupture of other proximate surface faults within Cook Strait (Holdgate and Grapes 2015). Coseismic submarine landslides have also been implicated as potentially contributing to the propagation and run-up of tsunami waves following the 1855 CE Wairarapa earthquake (Grapes and Downes 1997; Barnes 2005) with the side walls of the Cook Strait Canyon showing evidence of past landslides (Lane et al. 2016). Furthermore, the narratives from Ngāti Koata and Ngāti Kuia histories (King et al. 2018) as well as recently uncovered recollections from Farewell Spit (Supplementary data 7) suggest a more complex tsunamigenesis storyline across Cook Strait in 1855 CE. Consequently, we suggest that the generating sources of the 1855 CE tsunami should be re-examined, and/or that tsunami hazard in the outer parts of the Marlborough Sounds may be underestimated by existing tsunami models as there may be local complexities that lead to higher run-ups and amplification (i.e. wave resonance) than expected.

Based on the multi-proxy evidence and other contextual details presented in this study, we consider tsunami inundation in association with the rupture of the onshore-offshore Wairarapa fault in 1855 CE as the most likely emplacement mechanism for the marine deposit found at Swamp Bay. Linked to this interpretation, the very poorly sorted gravel and angular clasts that overly the marine deposit most likely represent alluvium and slope-wash from the surrounding hills loosened by ground-shaking in association with the 1855 CE earthquake, and transported soon after by fluvial processes on adjacent gully streams. Such interpretations are consistent with recent findings

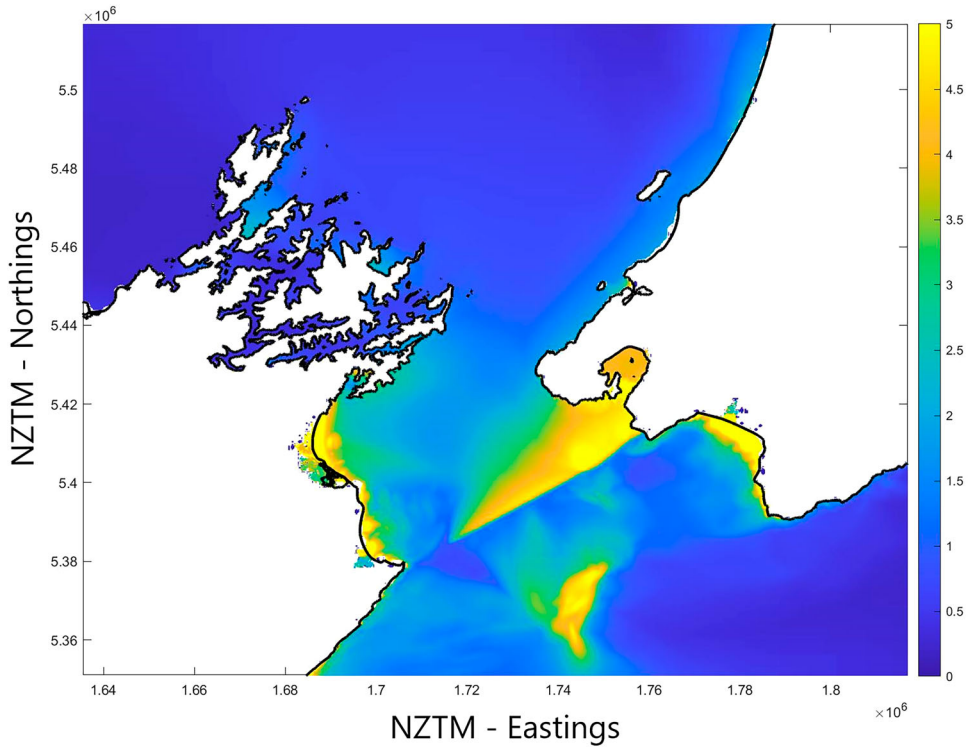

Figure 9. Modelled simulation of maximum tsunami heights across the Cook Strait region generated by the Wairarapa Fault in the 1855 CE Mw 8.2 earthquake. The colour scale shows the maximum increase in water level above the background level. Tsunami modelling was conducted using Basilisk (Popinet 2011; 2015) and the source model adapted from Mueller and Power (2014) for the earthquake deformation.

from Japan and Chile where both tsunami inundation and reworked sediments from surrounding catchments have entered the sedimentary record (Goff et al. 2016; Cisternas et al. 2017).

Importantly, this is not the first time that marine inundation signatures associated with the historical earthquake and tsunami of 1855 CE have been reported from the Cook Strait region, with previous studies undertaken at neighbouring sites - e.g. Abel Tasman National Park (Chagué-Goff and Goff 1999; Goff and Chagué-Goff 1999), Kapiti Island (Goff et al. 2000), and Mataora-Wairau Lagoon (King et al. 2017) (Figure 1). Nonetheless we acknowledge that research at other sites on Rangitoto ki te Tonga would help to test the tsunami origin hypothesis presented here as well as potentially locate older deposits possibly referred to in Ngāti Koata and Ngāti Kuia oral histories.

Conclusions

Informed by Māori oral histories that relate ancestral experience with past tsunami(s) across the top of the South Island, multi-proxy analysis indicates an anomalous sedimentary deposit across the north-eastern side of Swamp Bay, Rangitoto ki te Tonga (D'Urville Island). The deposit extends some 160 m inland of the present MHWM and includes two distinct lithofacies comprising a medium to coarse sand with discrete well-rounded pebbles and scattered plant rootlets overlain by a chaotic mixture of gravel and silts. Preserved between wetland mud below and soil at the surface the sand lithofacies coincide with increased percentages of benthic marine to brackish–marine diatom species as well as geochemical properties indicative of sudden changes in mineralogy. Radiocarbon dating indicates the deposit formation is less than 402 yrs BP, and pollen indicates it is very unlikely to be younger than 1870 CE. We infer from these multi-proxy data as well as contemporaneous deposits from neighbouring sites and documentary evidence that (i) the marine deposit was most likely emplaced by tsunami transport associated with rupture of the Wairarapa Fault in 1855 CE, and (ii) the overlying lithofacies of poorly sorted gravel and silts most likely represents slope-wash from the surrounding hills loosened by ground-shaking in association with the 1855 CE earthquake, and transported soon after by fluvial processes on adjacent gully streams. This study suggests the 1855 CE earthquake may have had a more complex source than previously thought and, or, available tsunami modelling for the Marlborough Sounds does not fully capture the local complexities in bathymetry and topography that can cause tsunami amplification in embayments like Swamp Bay. Further, this work is part of a greater project of acceptance of 'other' ways of knowing, and encourages plural ways of learning about tsunami hazard and risk.

Note

1. Although Aotearoa is a/one Māori name for New Zealand's North Island, Aotearoa–NZ is commonly used to refer to all of New Zealand.

Acknowledgements

The authors acknowledge Mr Gus Forgan (Patuki Station Farm) for permission to enter and survey Swamp Bay as well as Ngāti Koata Trust and Te Rūnanga o Ngāti Kuia for their involvement and support of this work. Dr Marcus Vandergoes is thanked for palynology advice, Jenny Dahl for helping with radiocarbon sample selection, and Dr William Power and Ms Gaye Downes for bringing our attention to the 1894 newspaper article about historic tsunami observations. Mr Arne Pallentin is thanked for his assistance with cartography and Ms Georgina Griffiths (MetService) is acknowledged for assistance with obtaining renders of mean sea level pressure analyses for the Aotearoa-NZ region during ex-tropical Cyclone Gita at the end of February 2018. Finally, we would like to acknowledge the two anonymous reviewers who provided constructive comments on an earlier version of the manuscript.

Disclosure statement

No potential conflict of interest was reported by the author(s).

Funding

This research was funded by the Resilience to Natures Challenges National Science Challenge – Vision Mātauranga Science Programme (grant agreement no. 28378), the NIWA Strategic Science Investment Fund – Hazards, Climate and Māori Society (grant agreement no.C01X1702), and the GNS Science It's Our Fault Programme (jointly funded by the Earthquake Commission, Wellington Regional Council and Wellington City Council).

Data availability statement

The supplementary data files that support the findings of this study are openly available in zenodo at https://doi.org/10.5281/zenodo.6585466.

ORCID

Catherine Chagué http://orcid.org/0000-0001-9330-8167
Emily Lane http://orcid.org/0000-0002-9261-6640
Daniel Hikuroa http://orcid.org/0000-0002-7340-7106
Shaun Williams http://orcid.org/0000-0003-3986-612X

References

Atwater B. 1987. Evidence for great Holocene earthquakes along the outer coast of Washington state. Science. 236:942–944. doi:10.1126/science.236.4804.942.

Atwater BF, Moore AL. 1992. A tsunami about 1000 years ago in Puget Sound. Washington. Science, 1614, 1614–1617. doi:10.1126/science.258.5088.1614

Barnes P. 2005. The southern end of the Wairarapa Fault, and surrounding structures in Cook strait. In: The 1855 Wairarapa Earthquake Symposium - Proceedings volume. Townend J, Langridge R, Jones, A, editors. Publication Number: GW/RINV-T-05/205. Wellington: Greater Wellington Regional Council; p. 66–71.

Barnes PM, Ghisetti FC. 2016. Structure, late quaternary slip rate and earthquake potential of marine reverse faults along the North Westland deformation front, New Zealand. New Zealand Journal of Geology and Geophysics. 59:157–175. doi:10.1080/00288306.2015.1112816.

Battarbee, RW. 1986. Diatom analysis. In: Handbook of holocene palaeoecology and palaeohydrology. Berglund BE, editors. Chichester: Wiley; p. 527–570.

Beavan J, Darby D. 2005. Fault slip in the 1855 Wairarapa earthquake based on new and reassessed vertical motion observations: did slip occur on the subduction interface? In: The 1855 Wairarapa Earthquake Symposium - Proceedings volume. Townend J, Langridge R, Jones A, editors. Publication Number: GW/RINV-T-05/205. Wellington: Greater Wellington Regional Council; p. 31–41.

Blott SJ, Pye K. 2001. Gradistat: a grain size distribution and statistics package for the analysis of unconsolidated sediments. Earth Surface Processes and Landforms. 26:1237–1248. doi:10.1002/esp.261.

Brailsford B. 1991. The tattooed land. Stoneprint Press, Wellington, 222 pp.

Bronk Ramsey C. 2009. Bayesian analysis of radiocarbon dates. Radiocarbon. 51(1):337–360. doi:10.1017/S0033822200033865.

Brownsey PJ, Smith-Dodsworth JC. 2000. New Zealand ferns and allied plants. Auckland: David Bateman. 168

Chagué C, Cope J, Kilroy C, Jacobsen G, Zawadzki A, Wong H. 2020. A 7300 year record of environmental changes in a coastal wetland (moawhitu), New Zealand, and evidence for catastrophic overwash (tsunami?). Sedimentary Geology. 407:1–17. doi:10.1016/j.sedgeo.2020.105746.

Chagué-Goff C. 2010. Chemical signatures of palaeotsunamis: a forgotten proxy? Marine Geology. 271:67–71. doi:10.1016/j.margeo.2010.01.010.

Chagué-Goff C, Chan JCH, Goff J, Gadd P. 2016. Late Holocene record of environmental changes, cyclones and tsunamis in a coastal lake, mangaia. Cook Islands. Island Arc. 25(5):333–349. doi.10.1111/iar.12153.

Chagué-Goff C, Goff J. 1999. Geochemical and sedimentological signature of catastrophic saltwater inundations (tsunami). New Zealand. Quaternary Australasia. 17:38–48.

Chagué-Goff C, Goff J, Wong HKY, Cisternas M. 2015. Insights from geochemistry and diatoms to characterise a tsunami's deposit and maximum inundation limit. Marine Geology. 359:22–34. doi:10.1016/j.margeo.2014.11.009.

Chagué-Goff C, Schneider J-L, Goff JR, Dominey-Howes D, Strotz L. 2011. Expanding the proxy toolkit to help identify past events — lessons from the 2004 Indian ocean tsunami and the 2009 south pacific tsunami. Earth-Science Reviews. 107:107–122. doi:10.1016/j.earscirev.2011.03.007.

Chagué-Goff C, Szczuciński W, Shinozaki T. 2017. Applications of geochemistry in tsunami research: a review. Earth-Science Reviews. 165:203–244. doi:10.1016/j.earscirev.2016.12.003.

Chawchai S, Kylander ME, Chabangborn A, Löwemark L, Wohlfarth B. 2016. Testing commonly used X-ray fluorescence core scanning-based proxies for organic-rich lake sediments and peat. Boreas. 45:180–189. doi:10.1111/bor.12145

Chester PI, Prior C. 2004. An AMS^{14}C pollen-dated sediment and pollen sequence from the late holocene, southern coastal Hawke's Bay, New Zealand. Radiocarbon. 46(2):721–731. doi:10.1017/S0033822200035761.

Cisternas M, Atwater BF, Torrejon F, Sawai Y, Machuca G, Lagos M, Eipert A, Toulton C, Saldago I, Kamataki T, et al. 2005. Predecessors of the giant 1960 Chile earthquake. Nature. 437:404–407. doi:10.1038/nature03943.

Cisternas M, Garrett E, Wessond R, Dura T, Ely LL. 2017. Unusual geologic evidence of coeval seismic shaking and tsunamis shows variability in earthquake size and recurrence in the area of the giant 1960 Chile earthquake. Marine Geology. 385:101–113. doi:10.1016/j.margeo.2016.12.007.

Clark KJ, Hayward BW, Cochran UA, Wallace LM, Power WL, Sabaa AT. 2015. Evidence for past subduction earthquakes at a plate boundary with widespread upper plate faulting: southern Hikurangi margin, New Zealand. Bulletin of the Seismological Society of America. 105(3):1661–1690. doi:10.1785/0120140291.

Clement AJH, Whitehouse PL, Sloss CR. 2016. An examination of spatial variability in the timing and magnitude of Holocene relative sea-level changes in the New Zealand archipelago. Quaternary Science Reviews. 131:73–101. doi:10.1016/j.quascirev.2015.09.025.

Cochran UA. 2002. Detection of large Holocene earthquakes in the sedimentary record of Wellington, New Zealand, using diatom analysis. Victoria University of Wellington, Wellington (303 pp, PhD Thesis).

Croudace IW, Rindby A, Rothwell RG. 2006. ITRAX: description and evaluation of a new X-ray core scanner. In: Rothwell RG, editor. New ways of looking at sediment cores and core data. London: Geological Society Special Publication; p. 51–63.

Dawson A, Long D, Smith DE. 1988. The storegga slides: evidence from eastern Scotland for a possible tsunami. Marine Geology. 82:271–276. doi:10.1016/0025-3227(88)90146-6.

Dawson AG, Shi S. 2000. Tsunami deposits. Pure and Applied Geophysics. 157:875–897. doi:10.1007/s000240050010.

De Martini PM, Barbano MS, Smedile A, Gerardi F, Pantosti D, Del Carlo P, Pirrotta C. 2010. A unique 4000 year long geological record of multiple tsunami inundations in the augusta Bay (eastern Sicily, Italy). Marine Geology. 276:42–57. doi:10.1016/j.margeo.2010.07.005.

Denys L, de Wolf H. 1999. Diatoms as indicators of coastal paleoenvironments and relative sea-level change. In: Stoermer E.F., Smol J.P, editor. The diatoms: applications for the environmental and earth sciences. Cambridge: Cambridge University Press; p. 277–297.

Downes G. 2015. New Zealand tsunami database: historical and modern records. GNS science, Lower. http://data.gns.cri.nz/tsunami/.

Dunbar GB, McLean W, Goff JR. 1997. Holocene pollen stratigraphy and sedimentation, Wellington harbour, New Zealand. New Zealand Journal of Geology and Geophysics. 40:325–333. doi:10.1080/00288306.1997.9514765.

Dura T, Hemphill-Haley E, Sawai Y. 2016. The application of diatoms to reconstruct the history of subduction

zone earthquakes and tsunamis. Earth-Science Reviews. 152:181–197. doi:10.1016/j.earscirev.2015.11.017.
Elliot MB, Striewski B, Flenley JR, Sutton DG. 1995. Palynological and sedimentological evidence for a radiocarbon chronology of environmental change and polynesian deforestation from Lake Taumatawhana, Northland, New Zealand. Radiocarbon. 37:899–916. doi:10.1017/S0033822200014983.
Faegri K, Iversen J, Kaland PE, Krzywinski K. 1989. Textbook of pollen analysis, 4th edition. Caldwell: The Blackburn Press. 328 pp.
Foged N. 1979. Diatoms in New Zealand, the North Island. Bibliotecha Phycologica. 47:1–130.
Goff J, Chagué-Goff C. 1999. A late Holocene record of environmental changes from coastal wetlands: Abel Tasman National Park, New Zealand. Quaternary International. 56:39-51.
Goff J, Chagué-Goff C, Nichol S, Jaffe B, Dominey-Howes D. 2012. Progress in palaeotsunami research. Sedimentary Geology. 243–244:70–88. doi:10.1016/j.sedgeo.2011.11.002
Goff J, Knight J, Sugawara D, Terry J. 2016. Anthropogenic disruption to the seismic driving of beach ridge formation: the Sendai Coast, Japan. Science of the Total Environment. 544:18–23. doi:10.1016/j.scitotenv.2015.11.106
Goff J, Rouse HL, Jones S, Hayward B, Cochran U, McLea W, Dickinson WW, Morley MS. 2000. Evidence for an earthquake and tsunami about 3100–3400 yr ago, and other catastrophic saltwater inundations recorded in a coastal lagoon, New Zealand. Marine Geology. 170:231–251. doi:10.1016/S0025-3227(00)00076-1.
Google-Earth-Pro. 2020. Swamp Bay, D'Urville Island; [accessed 10 November 2020]. https://earth.google.com/web.
Goto T, Satake K, Sugai T, Ishibe T, Harada T, Murotani S. 2015. Historical tsunami and storm deposits during the last five centuries on the Sanriku Coast, Japan. Marine Geology. 367:105–117. doi:10.1016/j.margeo.2015.05.009.
Grapes R, Downes G. 1997. The 1855 Wairarapa, New Zealand, earthquake. Bulletin of the New Zealand Society for Earthquake Engineering. 30:271–368.
Grunsky EC, Smee BW. 1999. The differentiation of soil types and mineralization from multi-element geochemistry using multivariate methods and digital topography. Journal of Geochemical Exploration. 67(1-3):287–299. doi:10.1016/S0375-6742(99)00054-0.
Guyard H, Chapron E, St-Onge G, Anselmetti FS, Arnaud F, Magand O, Francus P, Melieres MA. 2007. High-altitude varve records of abrupt environmental changes and mining activity over the last 4000 years in the western French Alps (Lake Bramant, Grandes Rousses Massif). Quaternary Science Reviews. 26:2644–2660. doi:10.1016/j.quascirev.2007.07.007.
Hartley B. 1996. An atlas of British diatoms. Bristol: Biopress Ltd. 601 pp.
Hemphill-Haley E. 1996. Diatoms as an aid in identifying late-Holocene tsunami deposits. The Holocene. 6 (4):439–448. doi:10.1177/095968369600600406.
Hogg AG, Heaton TJ, Hua Q, Palmer JG, Turney CSM, Southon J, Bayliss A, Blackwell PG, Boswijk G, Ramsey B, et al. 2020. Radiocarbon62 Southern Hemisphere calibration, 0–55,000 years cal BP. Radiocarbon. 62 (4):759–778. doi:10.1017/rdc.2020.59.
Holdgate GR, Grapes RH. 2015. Wairau basin and fault connections across Cook Strait, New Zealand: seismic and geological evidence. Australian Journal of Earth Sciences. 62(1):95–121. doi:10.1080/08120099.2015.986195.
Johnston MR. 1996. Geology of the D'Urville area. Institute of Geological & Nuclear Sciences Geological Map 16. Institute of Geological & Nuclear Sciences, Lower Hutt, 52 pp.
Kennedy DM, Risdon BV, Woods JDW. 2021. Holocene sea-level change and estuary infill in North West Nelson, central New Zealand. The Holocene. 32(3):113–126. doi:10.1177/09596836211060489.
Kershaw AP. 1997. A modification of the Troels-Smith system of sediment description and portrayal. Quaternary Australasia. 15:63–68.
King DN, Goff J, Chagué-Goff C, McFadgen BG, Jacobsen G, Gadd P, Horrocks M. 2017. Reciting the layers: evidence for past tsunamis at Mataora-Wairau Lagoon, Aotearoa-New Zealand. Marine Geology. 389:1–16. doi:10.1016/j.margeo.2017.05.001.
King DN, Shaw W, Meihana P, Goff J. 2018. Māori oral histories and the impact of tsunamis in Aotearoa-New Zealand. Natural Hazards and Earth System Sciences. 18:907–919. doi:10.5194/nhess-18-907-2018.
Krammer K, Lange-Bertalot H. 1986. Bacillariophyceae 1. Teil, Naviculaceae. – In: Ettl H, Gerloff J, Heynig H, & Mollenhauer D. (eds): Süßwasserflora von Mitteleuropa. 2 (1). G. Fischer, Stuttgart & New York, 876 pp.
Krammer K, Lange-Bertalot H. 1988. Bacillariophyceae 2. teil, bacillariaceae, epithemiaceae, surirellaceae. In: Ettl H, Gerloff J, Heynig H, Mollenhauer D, editors. Süßwasserflora von mitteleuropa. 2 (2). New York: G. Fischer, Stuttgart; 596 pp.
Krammer K, Lange-Bertalot H. 1991a. bacillariophyceae. 3. Teil: Centrales, Fragilariaceae, Eunotiaceae. – In: Ettl H, Gerloff J, Heynig H. & Mollenhauer D. (eds): Süßwasserflora von Mitteleuropa. 2 (3). G. Fischer, Stuttgart & Jena, 576 pp.
Krammer K, Lange-Bertalot H. 1991b. Bacillariophyceae. 4. Teil: Achnanthaceae. Kritische Ergänzungen zu Navicula (Lineolatae) und Gomphonema. Gesamtliteraturverzeichnis. Teil 1-4. – In: Ettl H, Gerloff J, Heynig H, & Mollenhauer D. (eds): Süßwasserflora von Mitteleuropa. 2 (4). G. Fischer, Stuttgart & Jena, 437 pp.
Lane EM, Mountjoy JJ, Power WL, Mueller C. 2016. Probabilistic hazard of tsunamis generated by submarine landslides in the Cook Strait canyon (New Zealand). Pure and Applied Geophysics. 173(12):3757–3774. doi:10.1007/s00024-016-1410-0.
McFadgen BG. 1982. Dating New Zealand archaeology by radiocarbon. New Zealand Journal of Science. 25:379–392.
McFadgen BG. 2007. Hostile shores: catastrophic events in pre-historic New Zealand and their impact on Maori coastal communities. Auckland: Auckland University Press. 298pp.
McFadgen BG, Goff JR. 2007. Tsunamis in the New Zealand archaeological record. Sedimentary Geology. 200:263–274. doi:10.1016/j.sedgeo.2007.01.007.
McGlone MS. 1989. The Polynesian settlement of New Zealand in relation to environmental and biotic changes. New Zealand Journal of Ecology. 12:115–129.
McGlone MS, Wilmshurst JM, Leach HM. 2005. An ecological and historical review of bracken (pteridium esculentum) in New Zealand, and its cultural significance. New Zealand Journal of Ecology. 29(2):165–184.
Minoura K, Nakaya S. 1991. Traces of tsunami preserved in inter-tidal lacustrine and marsh deposits: some examples from northeast Japan. The Journal of Geology. 99:265–287. doi:10.1086/629488.

Mitchell H, Mitchell J. 2004. Te Tau Ihu o te waka: a history of Maori of Marlborough and Nelson, volume. 1. Wellington: Huia Publishers. 500 pp.
Moar NT. 1993. Pollen grains of New Zealand dicotyledonous plants. Christchurch: Manaaki Whenua Press. 200 pp.
Monecke K, Finger W, Klarer D, Kongko W, McAdoo BG, Moore AL, Sudrajat SU. 2008. A 1000-year sediment record of tsunami recurrence in northern Sumatra. Nature. 455:1232–1234. doi:10.1038/nature07374.
Moore JG, Bryan WB, Ludwig KR. 1994. Chaotic deposition by a giant wave, Molokai, Hawaii. Geological Society of America Bulletin. 106:962–967. doi:10.1130/0016-7606(1994)106<0962:CDBAGW>2.3.CO;2.
Moore LB. 1955. The ecology of tussock grasslands. Proceedings of the New Zealand Ecological Society. 3:7–8.
Morton RA, Gelfenbaum G, Jaffe BE. 2007. Physical criteria for distinguishing sandy tsunami and storm deposits using modern examples. Sedimentary Geology. 200:184–207. doi:10.1016/j.sedgeo.2007.01.003.
Mueller C, Power WL. 2014. Hikurangi Subduction Zone and Wairarapa Fault Tsunami Source Models. GNS Science Consultancy Letter Report, CR 2014/246 LP, 12 pp.
Nicol A. 2011. Landscape history of the Marlborough Sounds, New Zealand. New Zealand Journal of Geology and Geophysics. 54(2):195–208. doi:10.1080/00288306.2010.523079.
Nodder SD, Lamarche G, Proust J-N, Stirling M. 2007. Characterizing earthquake recurrence parameters for offshore faults in the low-strain, compressional Kapiti-manawatu Fault system, New Zealand. Journal of Geophysical Research. 112(B12):1-25. doi:10.1029/2007JB005019.
Norris MW, Turnbull JC, Howarth JD, Vandergoes MJ. 2020. Pretreatment of terrestrial macrofossils. Radiocarbon, 62(2):349–360. doi:10.1017/RDC.2020.8.
Pascoe RM. 1983. The climate and weather of Marlborough. In: New Zealand Meteorological Service Miscellaneous Publication, 115 (12).
Patete A. 1997. D'Urville Island (Rangitoto ki te Tonga) in the northern South Island. Waitangi Tribunal Claims Report for the Northern South Island (Wai 102), Wellington, 241 pp.
Pocknall DT. 1981. Pollen morphology of the New Zealand species of *dacrydiumselander, podocarpus* L'Heritier, and *dacrycarpus endlicher* (podocarpaceae). New Zealand Journal of Botany. 19(1):67–95.
Popinet S. 2011. Quadtree-adaptive tsunami modelling. Ocean Dynamics. 61(9):1261–1285. doi:10.1007/s10236-011-0438-z.
Popinet S. 2015. A quadtree-adaptive multigrid solver for the Serre–Green–Naghdi equations. Journal of Computational Physics. 302:336–358. doi:10.1016/j.jcp.2015.09.009.
Ramírez-Herrera MT, Lagos M, Hutchinson I, Kostoglodov V, Machain ML, Caballero M, Giguitchaichvili A, Aguilar B, Chagué-Goff C, Goff J, et al. 2012. Extreme wave deposits on the Pacific coast of Mexico: tsunamis or storms? — A multi-proxy approach. Geomorphology. 139–140:360–371. doi:10.1016/j.geomorph.2011.11.002.
Reitz EJ, Shackley M. 2012. Environmental archaeology – manuals in archaeological method, theory and technique. New York: Springer; 560 pp.
Round FE, Crawford RM, Mann DG. 1990. The diatoms: biology and morphology of the genera. Cambridge: Cambridge University Press. 747 pp.
Smith SP. 1910. History and traditions of the Maoris of the west coast North Island of New Zealand prior to 1840. Memoirs of the Polynesian Society. 1:175–185.
Tanigawa K, Sawai Y, Namegaya Y. 2018. Diatom assemblages within tsunami deposits from the 2011 Tohoku-oki earthquake along the Misawa coast, Aomori Prefecture, northern Japan. Marine Geology. 396:6–15. doi:10.1016/j.margeo.2016.11.016.
Tuttle MP, Ruffman A, Anderson T, Hewitt J. 2004. Distinguishing tsunami from storm deposits in eastern North America: the 1929 Grand Banks tsunami versus the 1991 Halloween storm. Seismological Research Letters 75 Grand Banks tsunami versus the 1991 Halloween storm. Seismological Research Letters 75, 117–131. doi:10.1785/gssrl.75.1.117.
Van Dam H, Mertens A, Sinkeldam J. 1994. A coded checklist and ecological indicator values of freshwater diatoms from the Netherlands. Netherlands Journal of Aquatic Ecology. 28:117–133. doi:10.1007/BF02334251.
Vandergoes MJ, Howarth JD, Dunbar GB, Turnbull JC, Roop HA, Levy RH, Li X, Prior C, Norris M, Keller LD, et al. 2018. Integrating chronological uncertainties for annually laminated lake sediments using layer counting, independent chronologies and Bayesian age modelling (Lake Ohau, South Island, New Zealand). Quaternary Science Reviews. 188:104–120. doi:10.1016/j.quascirev.2018.03.015.
Vos PC, de Wolf H. 1993. Diatoms as a tool for reconstructing sedimentary environments in coastal wetlands; methodological aspects. Hydrobiologia. 269-270:285–296. doi:10.1007/BF00028027.
Wardle P. 1991. Vegetation of New Zealand. London: Cambridge University Press. 672 pp.
Webb, CJ, Sykes WR, Garnock-Jones, PJ. 1988. Flora of New Zealand Volume IV. Naturalised Pteridophytes, Gymnosperms, Dicotyledons. Christchurch: Botany division. Department of Scientific and Industrial Research. 672 pp.
Wellman HW. 1962. Maori occupation layers at D'Urville Island, New Zealand. New Zealand Journal of Geology and Geophysics. 5:55–73. doi:10.1080/00288306.1962.10420109.
Williams CA, Eberhart-Phillips D, Bannister BDHN, Henrys S, Reyners M, Sutherland R. 2013. Revised interface geometry for the Hikurangi subduction zone, New Zealand. Seismological Research Letters. 84(6):1066–1073. doi:10.1785/0220130035.
Witkowski A, Lange-Bertalot H, Metzeltin D. 2000. Diatom flora of marine coasts I. Iconographia Diatomologica, 7. A.R.G. Gantner Verlag K.G., Ruggell. 925 pp.
Woodward CA, Gadd PS. 2019. The potential power and pitfalls of using the X-ray fluorescence molybdenum incoherent: coherent scattering ratio as a proxy for sediment organic content. Quaternary International. 514:30–43. doi:10.1016/j.quaint.2018.11.031.
Yap W, Switzer AD, Gouramanis C, Marzinelli E, Wijaya W, Yan YT, Dominey-Howes D, Labbate M, Srinivasalu S, Jankaew K, Lauro FM. 2021. Environmental DNA signatures distinguish between tsunami and storm deposition in overwash sand. Communications Earth & Environment. 2:(129):1–15. doi:10.1038/s43247-021-00199-3.